Chapter 15
How *In Vivo* EPR Measures and Images Oxygen

Boris Epel, Gage Redler, and Howard J. Halpern

Abstract The partial pressure of oxygen (pO_2) in tissues plays an important role in the pathophysiology of many diseases and influences outcome of cancer therapy, ischemic heart and cerebrovascular disease treatments and wound healing. Over the years a suite of EPR techniques for reliable oxygen measurements has been developed. This is a mini-review of pulse EPR in vivo oxygen imaging methods that utilize soluble spin probes. Recent developments in pulse EPR imaging technology have brought an order of magnitude increase in image acquisition speed, enhancement of sensitivity and considerable improvement in the precision and accuracy of oxygen measurements.

Keywords EPR • Imaging • Oxygen • Relaxation

1 Spin Probe

The oxygen molecule has two unpaired electrons in a triplet state that exhibits very fast relaxation. Upon interaction with a paramagnetic spin probe, oxygen enhances the relaxation rate of the probe via Heisenberg exchange [1]. The Smoluchowski

B. Epel • G. Redler
Center for EPR Imaging In Vivo Physiology, Chicago, IL, USA

Department of Radiation Oncology, University of Chicago, Chicago, IL, USA

H.J. Halpern (✉)
Center for EPR Imaging In Vivo Physiology, Chicago, IL, USA

Department of Radiation Oncology, University of Chicago, Chicago, IL, USA

MC1105, Department of Radiation and Cellular Oncology, University of Chicago Medical Center, 5841 S. Maryland Ave, Chicago, IL 60637, USA
e-mail: h-halpern@uchicago.edu

H.M. Swartz et al. (eds.), *Oxygen Transport to Tissue XXXVI*, Advances in Experimental Medicine and Biology 812, DOI 10.1007/978-1-4939-0620-8_15,

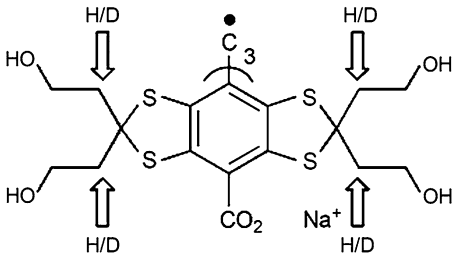

Fig. 15.1 Chemical structures of OX063 trityl

diffusion equation predicts a linear relationship between pO_2 and relaxation rates that is validated for multiple soluble radicals. This relationship allows a direct EPR measure of pO_2 with high precision [2].

The success of non-invasive oximetry in the last decade is strongly linked to triarylmethyl radicals or trityls (Fig. 15.1) developed by Nycomed Innovations (later acquired by GE Healthcare, Little Chalfont, Buckinghamshire, UK) possessing a narrow single EPR line [3]. The trityls that are commonly used for in vivo imaging are methyl-tris[8-carboxy-2,2,6,6-tetrakis[2-hydroxyethyl]benzo[1,2-d:4,5-d′]bis[1,3]dithiol-4-yl]-trisodium salt, OX063 (16 μT p-p) and its partially deuterated form Ox63H24D (8 μT p-p). These spin probes are distributed in the extracellular fluid compartment [2, 4]. In the blood stream of a mouse, the clearance halftime of these probes is approximately 9–10 min, whereas in tumors they remain and provide strong signals for about 40–50 min [5]. The lethal dose (LD50) of analogs of OX063 is very high, 8 mmol/kg, which allows high dose injections [6].

2 Imaging Methods

For imaging, the spatial position of a paramagnetic species is encoded by use of linear magnetic field gradients, **G**. The additional magnetic field experienced by a species at position **x** in the sample is then $\Delta B = \mathbf{G}\cdot\mathbf{x}$. The time evolution of signal from a sample after an RF pulse is

$$s(t) = \int_V f(x) exp\left(-\frac{t}{T_2^*(x)}\right) exp\left[-i2\pi k(t)x\right] dx \tag{15.1}$$

The time evolution of echoes can be treated in a similar way. Here, V describes an integral over the sample volume, and $\boldsymbol{f}(\boldsymbol{x})$ is the spatial distribution of the magnetization. The relaxation term $\exp\left(-\frac{t}{T_2^*(x)}\right)$ describes the attenuation of signal. The switching speed of the gradients achieved by EPR *in vivo* imaging hardware is slow in comparison to the relaxation rates of electrons (units of microseconds). Thus gradients constant on the time scale of spin probe relaxation are used in the definition of $\boldsymbol{k}$-space trajectories:

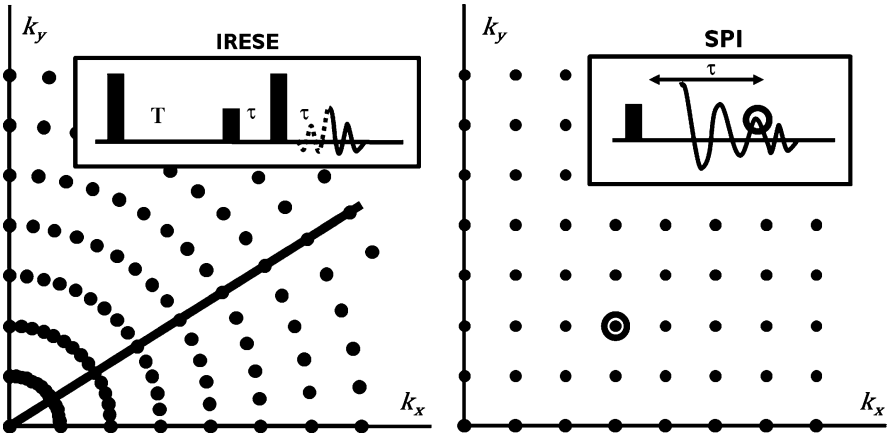

Fig. 15.2 Filling of two dimensional *k*-space by projection-based and single point imaging methods

$$k(t) == \frac{\gamma_e}{2\pi}\int_0^t G(t')dt' = \frac{\gamma_e}{2\pi}Gt. \tag{15.2}$$

For correct reconstruction of an image, sufficient *k*-space data must be acquired. Two general ways of filling *k*-space by using static gradients have been elaborated: projection-based and Fourier imaging.

2.1 Projection-Based Reconstruction

The gradient in (15.2) is a scaling factor between time and ***k***-values. By increasing of the gradient, the time, t, necessary to cover the desired k-space can be made small enough that the relaxation term in the (15.1) becomes negligible. In this case (15.1) describes the Radon transformation of an object in Fourier space along the direction defined by the gradient [7]. The ***k***-space trajectory of EPR signal detected under static gradient is a radial line passing through the origin of the *k*-space coordinates (Fig. 15.2). For spatial imaging, EPR projections are obtained while static gradients, **G**, with constant amplitude and different directions are applied. Different reconstruction algorithms have been developed for radially sampled data. Most of them fall into one of two categories: filtered back projection (FBP) [8, 9] or iterative reconstruction [10]. All reconstruction procedures on sparsely sampled data give inexact results: they represent a compromise between accuracy and the computation time required. FBP demands fewer computational resources, whereas iterative reconstruction generally produces fewer artifacts at a higher computing cost.

2.2 Single Point Imaging

The Single point imaging (SPI) method is based on phase encoding of spatial information. The method was originally used to overcome the influence of the EPR line width (or R_2*) on the imaging resolution [11]. Use of a single data point at delay $t=\tau$ (15.1) makes the relaxation term constant and allows for *k*-space sampling at will by choice of an appropriate static gradient. Typically, gradients are sampled on a rectangular grid (Fig. 15.2) and object [12, 13]. The object is then reconstructed by use of multidimensional Fourier transformation of *k*-space data.

SPI generates images free from artifacts at the expense of the necessity to repeat the measurement in every point of $\boldsymbol{k}$-space. Thus this method has higher spatial fidelity but somewhat lower SNR.

In the simplest form of SPI, free induction decay (FID) detection is used, and phase relaxation times are extracted from multiple images with different τ [12]. The disadvantage of this method is that, for a given set of gradients, the images reconstructed from different τ have different *k*-space samplings and, therefore, different spatial extents and resolutions. Resampling of these images to a common scale causes artifacts, especially around the edges of an object. More advanced sampling techniques that involve acquisition with use of multiple gradient grids have been suggested. This has led to the same *k*-space sampling for different τ and consequently the elimination of artifacts [13].

2.3 Pulse Sequences and 4D Images

Pulse sequences for measuring FID decay, spin-spin and spin-lattice (R_2^*, R_2 and R_1) relaxation are available. In all cases, the pulse sequence is chosen in a way that amplitude of the EPR signal time evolution becomes dependent on the relaxation time and sequence parameter (for example delay between pulses). Multiple 3D images with different values of this parameter are acquired and reconstructed independently. Then these images are stacked together to form 4D images, the additional dimension of which represents the evolution of signal amplitude in every voxel as a function of the sequence parameter. The final image of relaxation times is produced by fitting of this evolution to an appropriate dependence. This process is illustrated in Fig. 15.3 and resulting pO_2 image is presented in Fig. 15.4.

For SPI and single $\pi/2$-pulse, the fit of individual voxels to an exponential decay gives the FID decay rate R_2^*, related to R_2 as $R_2^* = \Sigma(R_2^i) + R_2$, where $\Sigma(R_2^i)$ is the sum of the known oxygen-independent contributions to R_2 [14].

For projection based imaging, the FID detection was not successful. Pulse imagers do not allow signal detection immediately after the excitation. The delay between excitation and opening of the detector (t_{dead}), leads to a missing volume in *k*-space, $\boldsymbol{k} < \gamma_e \mathbf{G} t_{dead,}$ and to image distortion.

To avoid incomplete coverage of *k*-space, projection-based pulse imaging techniques use dead time free spin echo sequences [15, 16]. The electron spin echo is detected by use of the two-pulse sequence $(\pi/2)$-τ-(π)-τ-echo; here, τ is the time

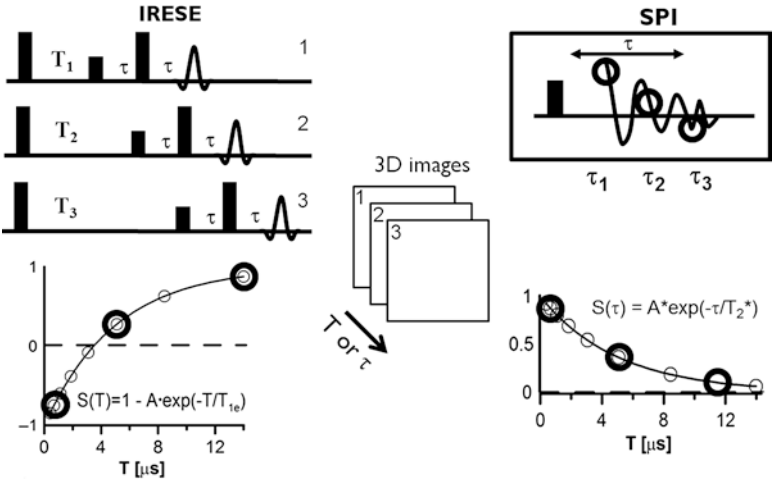

Fig. 15.3 Acquisition of 4D images

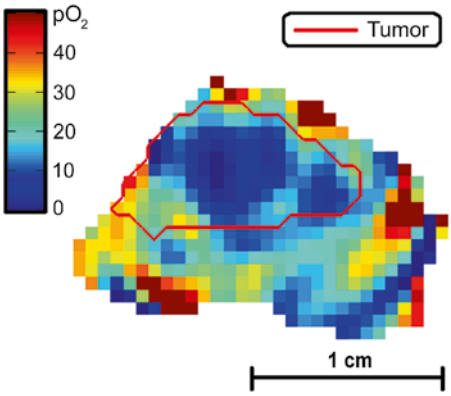

Fig. 15.4 R_1 pO_2 image of a murine leg with MCa4 F6 tumor. Sagittal slice with tumor outline obtained from MRI (*red*) is presented

delay between pulses. For acquiring of a phase relaxation image, separate images with different τ-delay values are obtained. These delays have to cover the range of times suitable for correct determination of the relaxation time. Logarithmically spaced delays yield a more precise determination of the relaxation time [16]. The echo sequence allow direct measurement of R_2, which results in higher pO_2 precision in comparison to R_2^* methods. Recently to obtain direct measurement of R_2 spin echo acquisition was introduced to SPI [17].

Finally, for generation of a spin-lattice relaxation (SLR) image, IRESE, the inversion recovery sequence (π)-T-(π/2)-τ-(π)-τ-echo can be used (Fig. 15.3) [18]. The first π-pulse inverts the populations of electron levels; the delay, T, allows this polarization to relax at the SLR rate. The detection sequence and imaging method are identical to that of the two pulse spin echo. The SLR images can be obtained using SPI as well.

3 Importance of Spin-Lattice Relaxation Imaging

Although oxygen-induced relaxation is the largest factor under physiologic conditions, other relaxation mechanisms can affect the accuracy of EPR oximetry. Some factors, such as temperature, viscosity, and salinity, are tightly controlled by a living body. Variations in these factors are relatively small and position-independent, so that their effects on relaxation rates can be accounted for. In contrast, spin-probe self-broadening, the effect of local spin-probe concentration on the relaxation rate, may be substantial and non-uniform and thus requires special treatment. Reducing trityl injection into the animal obviously reduces the trityl concentration *in vivo* and, thereby, the self-broadening. However, this strategy for reducing the self-broadening uncertainty in pO_2 also lowers the image SNR. These considerations stress the importance of a methodology that is less susceptible to concentration broadening. In trityls, the oxygen dependences of R_1 and R_2 are identical. However, the concentration dependence of R_2, especially at physiologic solvent salinity can be up to six times higher than that of R_1. Thus SLR measurement provides considerable improvement in the pO_2 image accuracy.

4 Conclusions

EPR oxygen imaging possesses the full suite of methods capable for accurate and precise imaging of small animals. This review is restricted to pulse EPR imaging. Continuous wave EPR also offers interesting oxygen imaging possibilities [19, 20].

Acknowledgments Supported by NIH grants P41 EB002034 and R01 CA98575.

References

1. Eastman PE, Kooser RG, Pas MR, Freed JH (1969) Studies of Heisenberg spin exchange in ESR spectra I. Linewidth and saturation effects. J Chem Phys 54(2690)
2. Tatum JL et al (2006) Hypoxia: Importance in tumor biology, noninvasive measurement by imaging, and value of its measurement in the management of cancer therapy. Int J Radiat Biol 82:699–757
3. Ardenkjaer-Larsen JH et al (1998) EPR and DNP properties of certain novel single electron contrast agents intended for oximetric imaging. J Magn Reson 133:1–12
4. Williams BB et al (2002) Imaging spin probe distribution in the tumor of a living mouse with 250 MHz EPR: correlation with BOLD MRI. Magn Reson Med 47:634–638
5. Matsumoto K et al (2004) Pharmacokinetics of a triarylmethyl-type paramagnetic spin probe used in EPR oximetry. Magn Reson Med 52:885–892
6. Krishna MC et al (2002) Overhauser enhanced magnetic resonance imaging for tumor oximetry: coregistration of tumor anatomy and tissue oxygen concentration. Proc Natl Acad Sci U S A 99:2216–2221

7. Williams BB, Pan XC, Halpern HJ (2005) EPR imaging: the relationship between CW spectra acquired from an extended sample subjected to fixed stepped gradients and the Radon transform of the resonance density. J Magn Reson 174:88–96
8. Deans SR (1983) The radon transformation and some of its applications. John Wiley & Sons, New York
9. Ahn KH, Halpern HJ (2007) Spatially uniform sampling in 4-D EPR spectral-spatial imaging. J Magn Reson 185:152–158
10. Ahmad R et al (2007) Enhanced resolution for EPR imaging by two-step deblurring. J Magn Reson 184:246–257
11. Maresch GG, Mehring M, Emid S (1986) High-resolution electron-spin-resonance imaging. Physica B C 138:261–263
12. Subramanian S et al (2002) Single-point (constant-time) imaging in radiofrequency Fourier transform electron paramagnetic resonance. Magn Reson Med 48:370–379
13. Devasahayam N et al (2007) Strategies for improved temporal and spectral resolution in in vivo oximetric imaging using time-domain EPR. Magn Reson Med 57:776–783
14. Matsumoto K et al (2006) Electron paramagnetic resonance imaging of tumor hypoxia: enhanced spatial and temporal resolution for in vivo pO(2) determination. Magn Reson Med 55:1157–1163
15. Mailer C, Sundramoorthy SV, Pelizzari CA, Halpern HJ (2006) Spin echo spectroscopic electron paramagnetic resonance imaging. Magn Reson Med 55:904–912
16. Epel B, Sundramoorthy SV, Mailer C, Halpern HJ (2008) A versatile high speed 250-MHz pulse imager for biomedical applications. Conc Magn Reson B 33B:163–176
17. Subramanian S et al (2012) Echo-based single point imaging (ESPI): a novel pulsed EPR imaging modality for high spatial resolution and quantitative oximetry (San Diego, CA: 1997). J Magn Reson 218:105–114
18. Epel B, Bowman MK, Mailer C, Halpern HJ (2013) Absolute oxygen R1e imaging in vivo with pulse electron paramagnetic resonance. Magnet Reson Med. Epub ahead of print
19. Gallez B, Baudelet C, Jordan BF (2004) Assessment of tumor oxygenation by electron paramagnetic resonance: principles and applications. NMR Biomed 17:240–262
20. Swartz HM, Clarkson RB (1998) The measurement of oxygen in vivo using EPR techniques. Phys Med Biol 43:1957–1975

Chapter 16
What We Learn from *In Vivo* EPR Oxygen Images

Gage Redler, Boris Epel, and Howard J. Halpern

Abstract Distributions of oxygen concentration (pO_2) are a critical determinant of normal tissue health as well as tumor aggressiveness and response to therapy. A number of studies show the value of normal tissue and tumor tissue oxygenation images and some of these will be discussed here. A strong correlation between tumor hypoxic fraction as measured with electron paramagnetic resonance oxygen imaging and radiation treatment success or failure has been found in two separate cancer types. Oxygen images of the torso of wild type mice show initial reduction of lung, liver, visceral, and muscle pO_2 with cyclic halving of fraction of inspired oxygen (FiO_2), but variation is blunted over an hour. Spontaneous breast cancers in Mouse Mammary Tumor Viral (MMTV) promoted-polyoma middle T antigen (PyMT) mice with BNIP3, a major factor in promotion of mitochondrial autophagy, knocked out will be compared with wild type animals. Preliminary studies for the BNIP3 knock out animals show extremely low pO_2. The wide variety of studies, in which oxygen images can play an integral role, serve to demonstrate the importance of oxygen images.

Keywords EPR • Oxygen imaging • Hypoxia • BNIP3 • Cancer • Microenvironment response

G. Redler • B. Epel
Center for EPR Imaging In Vivo Physiology, Chicago, IL, USA

Department of Radiation Oncology, University of Chicago, Chicago, IL, USA

H.J. Halpern (✉)
Center for EPR Imaging In Vivo Physiology, Chicago, IL, USA

Department of Radiation Oncology, University of Chicago, Chicago, IL, USA

MC1105, Department of Radiation and Cellular Oncology, University of Chicago Medical Center, 5841 S. Maryland Ave, Chicago, IL 60637, USA
e-mail: h-halpern@uchicago.edu

H.M. Swartz et al. (eds.), *Oxygen Transport to Tissue XXXVI*, Advances in Experimental Medicine and Biology 812, DOI 10.1007/978-1-4939-0620-8_16,

1 Introduction

In vivo oxygen concentration (pO_2) has been found to be crucially important in determining normal tissue health as well as the aggressiveness of tumors and their response to various forms of treatment [1–4]. Due to the ubiquitous influence of tissue pO_2 various methods for measuring and/or imaging pO_2 have been developed [5–8].

One such method is electron paramagnetic resonance (EPR) oxygen imaging (EPROI). EPROI is a particularly robust method of imaging in vivo tissue pO_2 distributions for several reasons. EPROI provides full 3D images of pO_2. These images have good spatial resolution (~1 mm^3 voxels) as well as pO_2 resolution (1–3 torr). The low electromagnetic wave excitation frequencies (e.g., 250 MHz) currently used in EPRI are comparable to those used in 6T whole body MRI and can penetrate deep in tissue (>7 cm) in animals as large as humans. EPROI images are obtained non-invasively, which means they can be used to study in vivo pO_2 distributions without perturbing the system. EPROI requires an intravenously injected, non-toxic spin probe, which distributes in the extracellular compartment of tumors, to report local pO_2 [9]. The accuracy of EPROI oxygen measurements has been established by correlating with well-established optical fiber based oxygen measurement techniques [10].The information provided by EPROI can be applied to help study myriad interesting oxygen related biologic and physiologic topics. A number of studies demonstrating the array of interesting applications of 3D EPR oxygen images of normal tissue and/or tumor tissue will be presented here.

2 Methods

EPROI is used to non-invasively determine the effect of tumor pO_2 on success of tumor treatment with radiation therapy. Two cancer models are used: fibrosarcoma (FSa) and murine mammary MCa4 carcinoma. Fraction of EPROI voxels with less than 10 torr pO_2 (HF10) is used as a measure of tumor hypoxia. The variable HF10 is then correlated to success or failure of radiotherapy to see what role, if any, hypoxia as determined by EPROI plays in tumor resistance to treatment.

EPROI has been used to provide insight into the effect of fraction of inspired oxygen (FiO_2) changes on the distribution of pO_2 in various organs of mice. The result of cyclic FiO_2 variation can also be observed in various organs using EPROI. This directly assesses levels of tissue pO_2 in models of important disorders such as sleep apnea to understand their biologic effects.

To examine the role of BNIP3 in tumor progression and regulation of oxygenation, changes in pO_2 levels and distributions in mouse mammary tumors are compared for BNIP3 null mice that have been crossed to the Mouse Mammary Tumor Viral (MMTV) promoted-polyoma middle T antigen (PyMT) mouse model of breast cancer and wild type mice. EPROI images are registered with anatomic CT images to analyse differences in oxygenation within these tumors.

3 Results

Using two cancer models (FSa and MCa4), we found that EPROI corroborates the theory that tumors exhibiting a higher degree of hypoxia tend to be more resistant to radiation therapy. A cohort of animals with either of the two tumor lines were treated to the previously determined 50 % tumor control dose (TCD_{50}) for each tumor type. The HF10 as determined by EPROI for each tumor was correlated with radiation therapy treatment outcome. For the FSa tumors, hypoxic tumors (HF10 > 10 %) 37 % were successfully controlled while for tumors with HF10 < 10 %, 90 % were successfully controlled ($p = 0.0138$) [11, 12]. For the MCa4 tumors, hypoxic tumors (HF10 > 10 %) 23 % were successfully controlled while for tumors with HF10 < 10 %, 90 % were successfully controlled ($p = 0.0072$) [12]. An example of the dramatic oxygenation difference observed in animals whose tumors were successfully controlled with radiotherapy versus those for which radiotherapy failed is shown in Fig. 16.1.

Significant differences in the overall pO_2 in three tissue types of a mouse breathing air versus a mouse breathing 12 % O_2 are seen in whole-body EPROI (Fig. 16.2). It is seen that significant variations in tissue pO_2 are observed with oscillating FiO_2, however the response becomes damped over time (Fig. 16.3). The direct assessment of tissue pO_2 responses in vivo provides data concerning the extent of hypoxia induced in these tissues and allows the development of models explaining the deleterious end organ effects.

Preliminary studies of BNIP3 knock out (KO) mice show extremely hypoxic breast tumors (Fig. 16.4). This is consistent with the fact that BNIP3 null tumor cells show increased invasive properties, suggesting that BNIP3 is a metastasis suppressor required to maintain mitochondrial integrity and mitigate against the metastasis promoting activities of reactive oxygen and hypoxia [13].

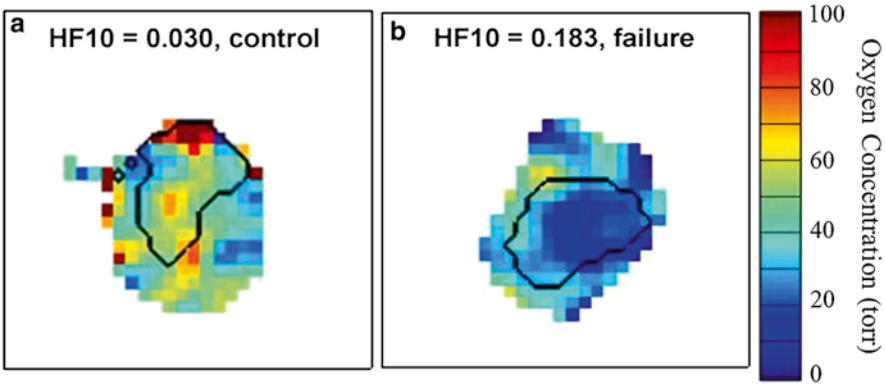

Fig. 16.1 Sample slices from representative EPROI of mouse legs bearing tumors (*black outline*) demonstrating the difference in tumor oxygenation observed in animals where treatment with radiation therapy eventually (**a**) successfully controlled the tumor or (**b**) failed to control the tumor

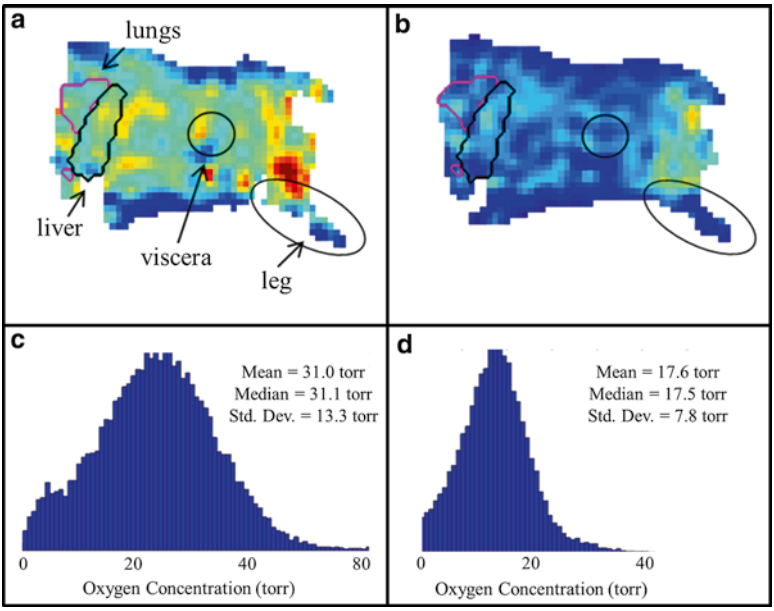

Fig. 16.2 Demonstration of the overall effect on the tissue pO_2 of a mouse when the breathing gas oxygen content is changed from 21 % O_2 to 12 % O_2 as measured with EPROI. Whole body EPROI of a mouse breathing (**a**) 21 % O_2 and (**b**) 12 % O_2, with labeled regions of interest. The pO_2 distributions for the whole body EPROI when the mouse is breathing (**c**) 21 % O_2 and (**d**) 12 % O_2

4 Discussion and Conclusions

With EPROI we can begin to develop quantitative assays of hypoxia induced in tumors and normal tissues. These, in turn will allow the development of quantitative models of the response of tumors and normal tissues to anti-cancer therapies and models of end-organ damage from disease processes such as the intermittent hypoxia induced by sleep apnea.

The hypoxic fraction of a tumor, as determined by EPROI, has been found to be quite a powerful determinant in the eventual outcome of treatment with radiation. This validates EPROI as a tool to analyze spatial distributions of pO_2 in vivo.

In preliminary studies EPROI has also proven to be a valuable tool for tracking tissue pO_2 response to changes in FiO_2. EPROI therefore has the potential to enhance studies investigating the biologic consequences of temporally fluctuating tissue oxygenations (e.g., sleep apnea conditions) by allowing noninvasive tracking of the response to FiO_2 changes of whole body pO_2 as well as pO_2 of individual organs and how this response changes over time.

EPR oxygen images can also help investigate the complicated effects of hypoxia on several aspects of tumor and tissue development. This is evidenced by preliminary results from a study investigating the effect of the BNIP3 protein, which limits

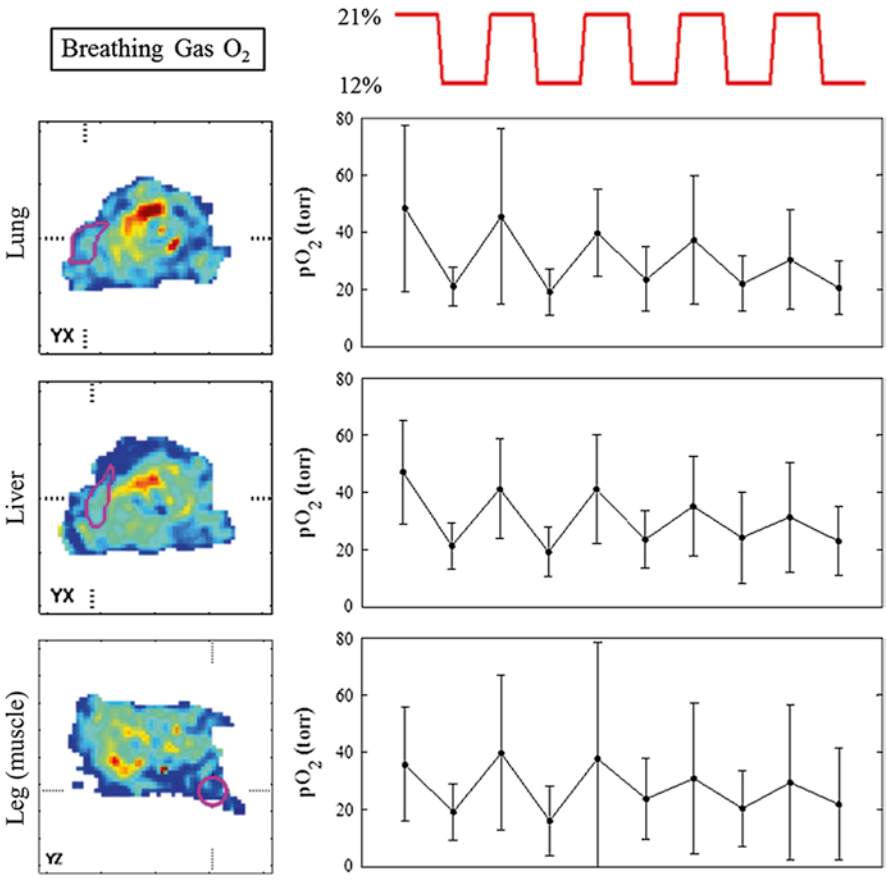

Fig. 16.3 Slices from an EPROI of a mouse are shown with regions of interest outlined in *magenta*. The breathing gas oxygenation for the mouse alternates from 21 % O_2 to 12 % O_2 (breathing gas O_2 changes shown in *red line*). Next to each image with a particular region of interest (lung, liver, or leg muscle) the change in mean oxygenation within that region of interest in response to the breathing gas change is shown

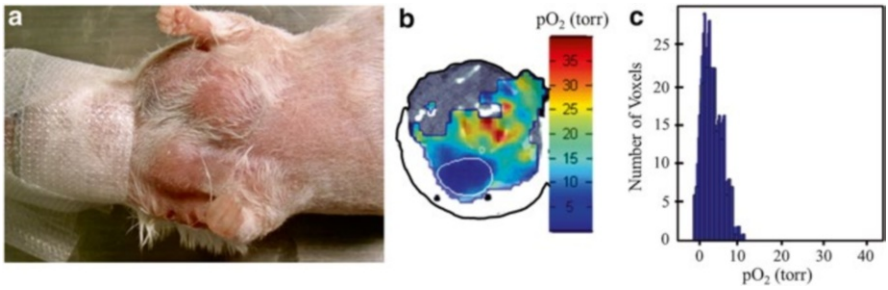

Fig. 16.4 (**a**) Photograph of MMTV-PyMT, BNIP3 null breast cancer tumors grown in the breast of a mouse. (**b**) Registered EPROI overlaid on an anatomical CT of the mouse, shown with the tumor outlined in *white*. (**c**) Distribution of pO_2 found within the BNIP3 null tumor demonstrating that the tumor is extremely hypoxic

production of reactive oxygen species by promoting mitochondrial degradation at the autophagosome, on tumor oxygenation. Initial results show that tumors in BNIP3 KO mice are extremely hypoxic, which may be due to dysfunctional mitochondria. EPROI will help in further studies to investigate the effect of BNIP3 on oxygenation as well as radiation resistance.

In general, oxygen images from EPROI provide an important tool in understanding the relationship between microenvironment oxygenation and a wide variety of crucial physiologic functions.

Acknowledgments Supported by NIH grants P41 EB002034 and R01 CA98575.

References

1. Hockel M, Schlenger K, Aral B et al (1996) Association between tumor hypoxia and malignant progression in advanced cancer of the uterine cervix. Cancer Res 56:4509–4515
2. Shannon AM, Bouchier-Hayes DJ, Condron CM et al (2003) Tumour hypoxia, chemotherapeutic resistance and hypoxia-related therapies. Cancer Treat Rev 29:297–307
3. Carmeliet P, Dor Y, Herbert JM et al (1998) Role of HIF-1alpha in hypoxia-mediated apoptosis. Nature 394:485–490
4. Rofstad EK (2000) Microenvironment-induced cancer metastasis. Int J Radiat Biol 76:589–605
5. Dewhirst MW, Klitzman B, Braun RD et al (2000) Review of methods used to study oxygen transport at the microcirculatory level. Int J Cancer 90:237–255
6. Zhao DW, Jiang L, Mason RP (2004) Measuring changes in tumor oxygenation. Methods Enzymol 386:378–418
7. Tatum JL (2006) Hypoxia: importance in tumor biology, noninvasive measurement by imaging, and value of its measurement in the management of cancer therapy. Int J Rad Biol 82:699–757
8. Bayer C, Vaupel P (2012) Acute versus chronic hypoxia in tumors: controversial data concerning time frames and biological consequences. Strahlenther Onkol 188:616–627
9. Golman K, Petersson JS, Ardenkjaer-Larsen JH et al (2000) Dynamic in vivo oxymetry using overhauser enhanced MR imaging. J Magn Reson Imaging 12:929–938
10. Elas M, Ahn KH, Parasca A et al (2006) Electron paramagnetic resonance oxygen images correlate spatially and quantitatively with oxylite oxygen measurements. Clin Cancer Res 12:4209–4217
11. Elas M, Bell R, Hleihel D et al (2008) Electron paramagnetic resonance oxygen image hypoxic fraction plus radiation dose strongly correlates with tumor cure in FSa fibrosarcomas. Int J Radiat Oncol Biol Phys 71:542–549
12. Elas M, Magwood JM, Butler B et al (2013) EPR oxygen images predict tumor control by a 50 percent tumor control radiation dose. Cancer Res (online and in press)
13. Tracy K, Macleod KF (2007) Regulation of mitochondrial integrity, autophagy and cell survival by BNIP3. Autophagy 3(6):616–619

Chapter 17
EPR Image Based Oxygen Movies for Transient Hypoxia

Gage Redler, Boris Epel, and Howard J. Halpern

Abstract Chronic hypoxia strongly affects the malignant state and resistance to therapy for tumors. Transient hypoxia has been hypothesized, but not proven to be more deleterious. Electron paramagnetic resonance imaging (EPRI) provides non-invasive, quantitative imaging of static pO_2 in vivo. Dynamic EPRI produces pO_2 movies, enabling non-invasive assessment of in vivo pO_2 changes, such as transient hypoxia. Recent developments have been made to enable Dynamic EPRI. Maximally spaced projection sequencing has been implemented to allow for more accurate and versatile acquisition of EPRI data when studying dynamic systems. Principal component analysis filtering has been employed to enhance SNR. Dynamic EPRI studies will provide temporally resolved oxygen movies necessary to perform in vivo studies of physiologically relevant pO_2 changes in tumors. These oxygen movies will allow for the localization/quantification of transient hypoxia and will therefore help to disentangle the relationship between chronic and transient hypoxia, in order to better understand their roles in therapeutic optimization and outcome.

Keywords Dynamic EPRI • Oxygen movies • PCA • Projection acquisition • Transient hypoxia

G. Redler • B. Epel
Center for EPR Imaging In Vivo Physiology, Chicago, IL, USA

Department of Radiation Oncology, University of Chicago, Chicago, IL, USA

H.J. Halpern (✉)
Center for EPR Imaging In Vivo Physiology, Chicago, IL, USA

Department of Radiation Oncology, University of Chicago, Chicago, IL, USA

MC1105, Department of Radiation and Cellular Oncology, University of Chicago Medical Center, 5841 S. Maryland Ave, Chicago, IL 60637, USA
e-mail: h-halpern@uchicago.edu

H.M. Swartz et al. (eds.), *Oxygen Transport to Tissue XXXVI*, Advances in Experimental Medicine and Biology 812, DOI 10.1007/978-1-4939-0620-8_17,

1 Introduction

The important prognostic implications related to the oxygenation status of tumors have been known for decades [1]. Chronic hypoxia, or chronically low oxygen concentration (pO_2), results in greater resistance to radiation therapy for cancer cells [2, 3] and therefore has been correlated with radiotherapy treatment failure in humans [4]. Additionally, tumors exhibiting chronic hypoxia are more resistant to chemotherapy [5], tend to grow more rapidly due to abnormal proliferation [6], and have increased potential for metastatic progression [7]. These implications have led to a high level of interest in methods for measuring/imaging pO_2 deep in tissues.

Diffusion limited chronic hypoxia was the first form of hypoxia found in tumors [8] and for many years was believed to be the only type of hypoxia present in tumors. However, more recent studies have found that perfusion limited transient hypoxia is present as well [9–12] and may even be the major cause of hypoxia in tumours [12, 13]. Studies suggest that transient hypoxia may be as important a determinant of cancer progression and patient prognosis as chronic hypoxia, if not more important. However, currently no definitive conclusions can be made due to inconsistencies in the data and methodological approaches from previous studies investigating the biologic effects of transient hypoxia versus those of chronic hypoxia. Furthermore, lack of data correlating a quantitative measure of transient hypoxia in vivo with treatment outcome currently precludes such a comparison [14].

Electron paramagnetic resonance imaging (EPRI) has proven to be a robust imaging modality for studying tissue pO_2 in vivo. EPRI noninvasively acquires highly-resolved, both spatially (~1 mm^3 voxels) and in pO_2 (1–3 torr), 3D images of pO_2 in vivo [15–19]. Acquisition time for our standard EPRI is on the order of 10 min, which is suitable for studying chronic hypoxia.

However, in order to use EPRI to study transient hypoxia, recent developments have been made to allow for improvements in temporal resolution (acquisition time on the order of 1 min) and accuracy. A novel acquisition method for maximally spaced projection sequencing has been implemented to allow for more accurate and versatile acquisition of EPRI data when studying dynamic systems (e.g., transient hypoxia). Principal component analysis (PCA) filtering has been employed as well to enhance SNR and thus allow for improved temporal resolution. These improvements enable Dynamic EPRI, which can provide 4D EPRI based oxygen movies and allow for the necessary non-invasive studies investigating transient hypoxia to eventually help determine its biologic implications.

2 Methods

2.1 Maximally Spaced Projection Sequencing

EPRI is a projection based imaging modality. Linear fixed magnetic field gradients are applied in a spherical geometry to spatially encode a 3D object. This enables the acquisition of projections of the object along the direction of the applied gradient.

With a sufficient number of these projections an image of the object can be reconstructed using an inverse radon transform. A series of 3D images with varying pulse sequence parameters is acquired, enabling a voxel-by-voxel fit of signal relaxation to determine T_1 and/or T_2, which provides a measure of local pO_2 at each voxel [22]. The rapidity with which these can be acquired is proportional to the number of projections acquired for each image and the speed at which each projection is acquired. Both the number and uniformity of acquired projections influence the image quality. More uniformly distributed projections provides more efficient data acquisition, i.e. relatively higher quality images can be reconstructed from smaller numbers of projections when they are more uniformly distributed. The influence of the uniformity of the spatial distributions of projections has been extensively studied [20, 21], but the uniformity with which the projections are acquired can still be optimized.

The directions through which projections are acquired can be represented as points on the unit sphere (unit hemisphere sufficient due to radon transform symmetry). Until now, a polar azimuthal raster (PAR) method has been used to acquire projections. The PAR method rasters through projection points on one side of the unit hemisphere and then back down the other, resulting in non-uniform distributions of projections throughout image acquisition. A new maximally spaced projection sequencing (MSPS) method has been implemented to achieve more uniform acquisition of projections. For the MSPS method, successive projections are acquired so that they are maximally spaced from projections that have already been acquired. In order to ensure uniformity for the final image, projection points are chosen from some final set of uniformly distributed points.

2.2 Principal Component Analysis Filtering

Principal component analysis (PCA) is a method for defining a new orthonormal basis on which to express some given n-D data set. The basis vectors, or principal components (PCs), are chosen to be the eigenvectors of the covariance matrix for the data. A subset of PCs span a smaller q-D space and contain mostly correlated features, while the space spanned by the other PCs contains mostly uncorrelated noise. Filtering of the data can be achieved with a low-order approximation by projection onto the subset of q PCs, thus selectively retaining relevant temporal patterns while discarding unwanted noise. PCA filtering is applied to dynamic EPRI studies as a pre-reconstruction spatiotemporal filter for projection data [22].

3 Results

3.1 Maximally Spaced Projection Sequencing

The distribution of projections at intermediate steps throughout imaging converge to uniformity more rapidly for the MSPS method as successive projections are acquired than for the PAR method. This yields intermediate images reconstructed

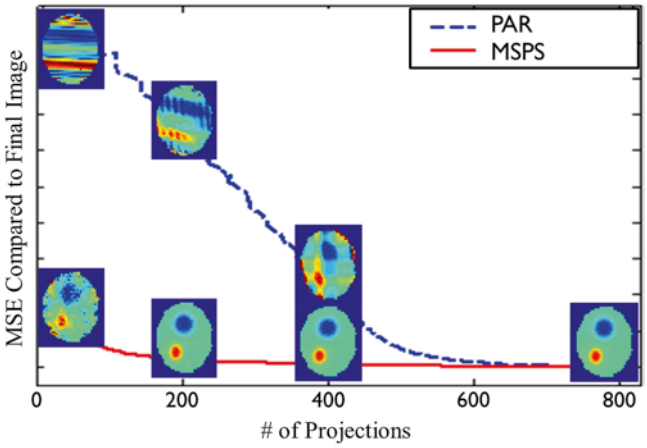

Fig. 17.1 Uniformly distributed projections throughout imaging for the MSPS method results in intermediate images that approximate the final image more rapidly than for the PAR method

from incomplete projection sets that approximate the final image more closely and earlier during imaging (Fig. 17.1).

The MSPS method affords the versatility to adjust temporal resolution to best fit the experiment and data following acquisition. This can be done simply by reconstructing temporally adjacent intermediate subsets of projections. These projection subsets are uniformly distributed enabling reconstruction of images of acceptable quality more rapidly than if a full set of projections is required. This allows for the visualization of important physiologic temporal changes that may not have been resolved with the temporal resolution of the original study (Fig. 17.2).

3.2 Principal Component Analysis Filtering

Simulation studies show that PCA filtering can significantly enhance SNR (by a factor of 3.8 ± 0.6) and allow for the order of magnitude improvement in temporal resolution necessary to obtain EPRI oxygen movies with 1 min frames (Fig. 17.3). PCA also helps to emphasize relevant temporal features. PCA is suited for data with large portions having common features and a small number of such features. Studies suggest that this is the case for tumors exhibiting transient hypoxia [22]. PCA filtering of Dynamic EPRI data is demonstrated in an experiment with a mouse breathing air (21 % O_2) followed by carbogen (95 % O_2) and then air again. One minute frames from this experiment are displayed and the tissue response to breathing gas changes can be clearly resolved.

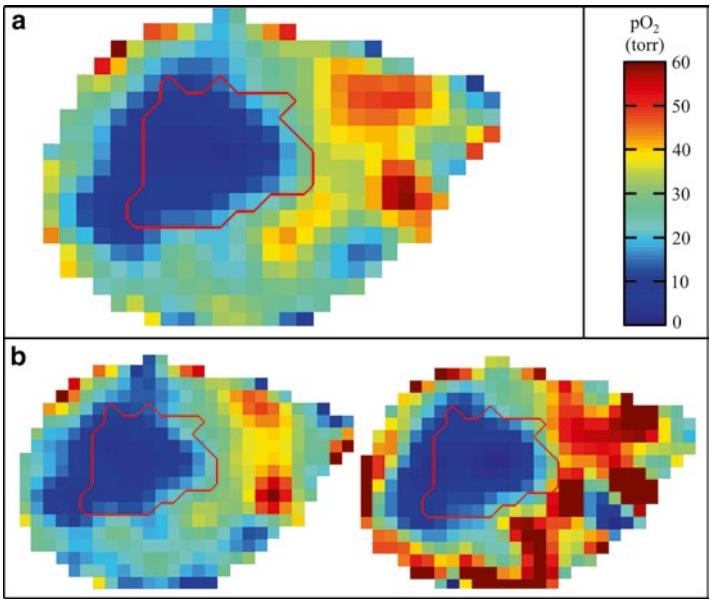

Fig. 17.2 (**a**) Single MSPS image acquired over 36 min with mouse breathing air for the first 18 min followed by carbogen for the second 18 min. (**b**) Two 18-min intermediate images that are subdivisions of the full image that now allow resolution of tissue response to increased breathing gas oxygen (tumor outlined in *red*)

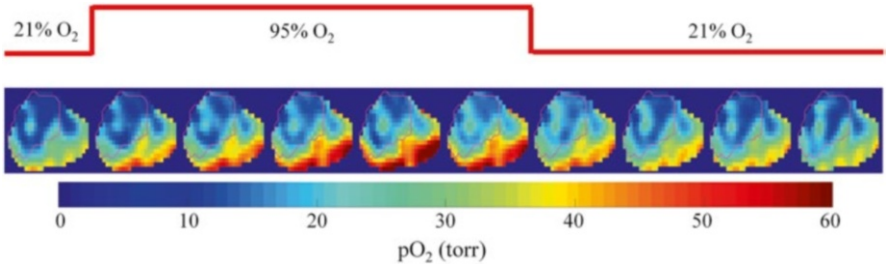

Fig. 17.3 One-minute frames from a PCA filtered Dynamic EPRI oxygen movie. Corresponding changes in breathing gas shown with *red line*. The mouse starts off breathing air and is switched to carbogen and then back to air. The temporal changes in tissue (tumor outlined in *red*) pO_2 are clearly resolved with such EPRI based oxygen movies

4 Discussion and Conclusions

Important tools such as the MSPS acquisition method and PCA filtering have been developed for EPRI in order to enable Dynamic EPRI with temporal resolution on the order of 1 min. PCA filtering of projection subsets acquired using the MSPS

method must be done carefully to avoid misrepresentation of projection differences due to varying projection views from subset to subset being considered as real pO_2 changes. PCA filtering of the full set of projections prior to subdivision can be done but may require a higher number of PCs to be included in the approximation, which will include more noise, and may not retain features with the higher temporal resolution afforded from reconstruction of sub-images. Another method requires a series of images acquired using MSPS, each of which can be subdivided to increase temporal resolution. The corresponding projection subsets can then each be grouped and separately PCA filtered.

The enhancements and versatility provided from the techniques discussed enable 4D EPRI based oxygen movies well resolved spatially, temporally, and in pO_2. Dynamic EPRI therefore is an ideal modality to study physiologically relevant temporal pO_2 changes in vivo without perturbing the system of interest. These oxygen movies will allow for the spatial localization as well as quantification (frequency, amplitude, etc.) of transient hypoxia in vivo and therefore enable the eventual determination of its clinical relevance.

Acknowledgments Supported by NIH grants P41 EB002034 and R01 CA98575.

References

1. Overgaard J (2007) Hypoxic radiosensitization: adored and ignored. J Clin Oncol 25:4066–4074
2. Schwarz G (1909) Uber Desensibilisierung gegen Rontgen-und Radiumstrahlen. Munch Med Wochenschr 56:1217
3. Hall EJ (2000) Radiobiology for the radiologist, 5th edn. Lippincott Williams & Wilkins, Philadelphia, PA
4. Hockel M, Schlenger K, Aral B et al (1996) Association between tumor hypoxia and malignant progression in advanced cancer of the uterine cervix. Cancer Res 56:4509–4515
5. Shannon AM, Bouchier-Hayes DJ, Condron CM et al (2003) Tumour hypoxia, chemotherapeutic resistance and hypoxia-related therapies. Cancer Treat Rev 29:297–307
6. Carmeliet P, Dor Y, Herbert JM et al (1998) Role of HIF-1alpha in hypoxia-mediated apoptosis, cell proliferation and tumour angiogenesis. Nature 394:485–490
7. Rofstad EK (2000) Microenvironment-induced cancer metastasis. Int J Radiat Biol 76:589–605
8. Thomlinson RH, Gray LH (1955) The histological structure of human lung cancers and the possible implications for radiotherapy. Br J Radiol 9:539–563
9. Brown JM (1979) Evidence for acutely hypoxic cells in mouse tumours, and a possible mechanism of reoxygenation. Br J Radiol 52:650–656
10. Chaplin DJ, Olive PL, Durand RE (1987) Intermittent blood-flow in a murine tumor – radiobiological effects. Cancer Res 47:597–601
11. Trotter MJ, Chaplin DJ, Olive PL (1991) Possible mechanisms for intermittent blood-flow in the murine SCCVII carcinoma. Int J Rad Biol 60:139–146
12. Durand RE, Lepard NE (1995) Contribution of transient blood-flow to tumor hypoxia in mice. Acta Oncol 34:317–323
13. Rofstad EK, Galappathi K, Mathiesen B et al (2007) Fluctuating and diffusion-limited hypoxia in hypoxia-induced metastasis. Clin Cancer Res 13:1971–1978
14. Bayer C, Vaupel P (2012) Acute versus chronic hypoxia in tumors: controversial data concerning time frames and biological consequences. Strahlenther Onkol 188:616–627

15. Elas M, Ahn KH, Parasca A et al (2006) Electron paramagnetic resonance oxygen images correlate spatially and quantitatively with oxylite oxygen measurements. Clin Cancer Res 12:4209–4217
16. Epel B, Sundramoorthy SV, Mailer C et al (2008) A versatile high speed 250 MHz pulse imager for biomedical applications. Concept Magn Reson B 33B:163–176
17. Epel B, Sundramoorthy SV, Barth ED et al (2011) Comparison of 250 MHz electron spin echo and continuous wave oxygen EPR imaging methods for in vivo applications. Med Phys 38:2045–2052
18. Epel B, Haney CR, Hleihel D et al (2010) Electron paramagnetic resonance oxygen imaging of a rabbit tumor using localized spin probe delivery. Med Phys 37:2553–2559
19. Elas M, Williams BB, Parasca A et al (2003) Quantitative tumor oxymetric images from 4D electron paramagnetic resonance imaging (EPRI): methodology and comparison with blood oxygen level-dependent (BOLD) MRI. Magn Reson Med 49:682–691
20. Ahmad R, Deng YM, Vikram DS et al (2007) Quasi Monte Carlo-based isotropic distribution of gradient directions for improved reconstruction quality of 3D EPR imaging. J Magn Reson 184:236–245
21. Ahmad R, Vikram DS, Clymer B et al (2007) Uniform distribution of projection data for improved reconstruction quality of 4D EPR imaging. J Magn Reson 187:277–287
22. Redler G, Epel B, Halpern HJ (2013) Principal component analysis enhances SNR for dynamic electron paramagnetic resonance oxygen imaging of cycling hypoxia in vivo. Magn Reson Med (unpublished)